

Tunneling Field-Effect Junctions with WS_2 barrier

Xiang-Guo Li, Yun-Peng Wang, X.-G. Zhang, and Hai-Ping Cheng*

Department of Physics and Quantum Theory Project, University of Florida, Gainesville, FL

32611

E-mail: cheng@qtp.ufl.edu

Phone: (+1)352-392-6256. Fax: (+1)352-392-8722

Abstract

Transition metal dichalcogenides (TMDCs), with their two-dimensional structures and sizeable bandgaps, are good candidates for barrier materials in tunneling field-effect transistor (TFET) formed from atomic precision vertical stacks of graphene and insulating crystals of a few atomic layers in thickness. We report first-principles study of the electronic properties of the Graphene/ WS_2 /Graphene sandwich structure revealing strong interface effects on dielectric properties and predicting a high ON/OFF ratio with an appropriate WS_2 thickness and a suitable range of the gate voltage. Both the band spin-orbit coupling splitting and the dielectric constant of the WS_2 layer depend on its thickness when in contact with the graphene electrodes, indicating strong influence from graphene across the interfaces. The dielectric constant is significantly reduced from the bulk WS_2 value. The effective barrier height varies with WS_2 thickness and can be tuned by a gate voltage. These results are critical for future nanoelectronic device designs.

Introduction

Performance of electronic and optoelectronic devices is fundamentally linked to the physical properties of materials that make them. The link between device performance and consequences of

quantum physics becomes increasingly direct and apparent as devices are scaled to the nanometer range and low dimensions. A primary example is the direct link between the band structure of semiconductors and their abilities to absorb and emit light.¹ The direct to indirect band gap change for few layer transition metal dichalcogenides (TMDCs), for example, combined with strong spin-orbit coupling and valley interactions,²⁻⁴ provides tremendous potential for coupling optical, spin, and valley electronics in these materials. TMDCs have been studied by researchers for decades for their electronic, optical, mechanical, and thermal properties.⁵⁻⁸ Recent advances in sample preparation, optical detection, transfer and manipulation of 2D materials have paved the way for their use in new field effect transistor (FET) and optoelectronic device designs. In addition to the change in band gap as a function of number of atomic layers, other properties of TMDC materials may also be dependent on their thickness. The dielectric constant of few-layer In_2Se_3 nanoflakes has been found to be dependent on the thickness.⁹ Band splitting in TMDCs due to spin-orbit coupling, on the other hand, was found to be less sensitive to their thickness.¹⁰ How these properties are impacted by contacting to graphene electrodes in a vertical tunnel junction structure under different layer thicknesses is an open question.

Another example of the direct impact of quantum mechanics on electronics performance is the ON/OFF ratio, the ratio of the electric current through a FET between its “ON” state and its “OFF” state and one of the key performance parameters of the device. This ratio is fundamentally controlled by the band gap and the carrier mobility of the channel material. Such link is accentuated by new two-dimensional materials represented by graphene. Early planar graphene-based FET¹¹ suffered from a small ON/OFF ratio (less than a factor of 10) due to the absence of a band gap in graphene. Engineering a band gap in graphene using nanostructuring,¹²⁻¹⁴ chemical functionalization,^{15,16} or bilayer graphene^{17,18} adds complexity and degrades graphene’s electronic quality. An alternative graphene-based transistor architecture is a vertical tunneling field effect transistor (TFET).¹⁹ It relies on quantum tunneling^{20,21} through a thin insulator barrier inserted between two graphene sheets. The performance of the TFET, in particular its ON/OFF ratio, depends critically on the effective tunnel barrier height. The 2D hexagonal boron nitride (*h*-BN) has a band gap and

can be easily transferred on top of graphene, but its large band gap makes a high effective tunnel barrier that prevents the device from reaching the fully ON state, limiting the ON/OFF ratio¹⁹ to less than about 50.

Several 2D TMDCs such as WS₂ and MoS₂ with band gaps around 1-2 eV^{1,22,23} have been experimentally demonstrated to yield ON/OFF ratios exceeding 10⁶ when used as atomic thin tunnel barrier layers.²⁴ That a moderate band gap of 1-2 eV can yield such a high ON/OFF ratio contrasts sharply with all-graphene FETs without a band gap and TFETs with a large band gap both of which have very low ON/OFF ratios. Moreover, the TMDCs are known for their “soft” band gaps that can be changed easily via externally controlled parameters,^{25–27} for example via the gate voltage and the barrier layer thickness. Understanding how the band gaps and the barrier potential change with the gate voltage and the layer thickness will provide us with both physical insight of these materials and guidance for how to use them in device design.

These questions are answered through a series of density-functional theory (DFT)²⁸ calculations, in which we study the size (number of atomic layers of WS₂) and gate voltage dependences of the band splitting due to spin-orbit coupling, the dielectric constant, and the effective tunnel barrier in Graphene/WS₂/Graphene (Gr/WS₂/Gr) sandwich structures. To relate first-principles calculations with experimental observations, we combine the first-principles electronic structure calculations with a tunneling transport model to obtain the ON/OFF ratio and the current-voltage characteristics of the junction.

Theoretical Model and Computational Details

First-principles electronic structure calculations are performed based on the Perdew-Burke-Ernzerhof (PBE) exchange correlation functional to the density functional theory (DFT)²⁸ as implemented in the Quantum-Espresso package.²⁹ We employ fully relativistic projector-augmented-wave (PAW) pseudopotentials^{30,31} including spin-orbit coupling and a plan-wave basis with the cutoff energy of 60 Ry. For structural relaxation, the optimized exchange van der Waals functional B86b of Becke

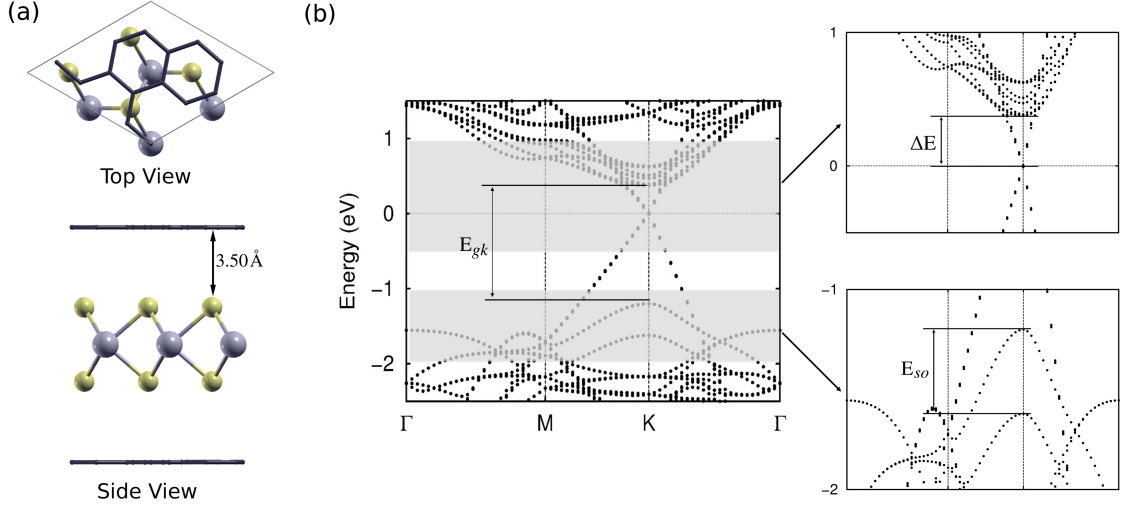


Figure 1: Geometrical and band structure of Gr/WS₂/Gr hybrid system. **(a)** Schematic top and side views of a hybrid Gr/WS₂/Gr sandwich with a monolayer of WS₂. **(b)** Band structure of Gr/monolayer WS₂/Gr system along high symmetric points Γ -M-K- Γ of 2×2 WS₂ supercell. Two shaded energy intervals are magnified in the panels on the right.

(opt B86b vdW) functional³² is chosen to include vdW interaction. The convergence thresholds for energy and force are 10^{-8} Ry and 0.0015 Ry/ \AA , respectively. A combination of $40 \times 40 \times 1$ and $6 \times 6 \times 1$ k -point samplings are applied for single-point energy and structure relaxation calculations, respectively. The gate field is applied using the effective screening medium (ESM) method³³ as implemented in Ref. 34. Technically, the gate field is created by adding a suitable extra electrons or holes to Gr/WS₂/Gr since the areal density of free carriers is proportional to the gate voltage.³⁴ To simulate a Gr/WS₂/Gr sandwich structure, we consider an S-terminated surface of WS₂ with a triangular lattice of S atoms at the topmost and bottommost layers. A supercell, with a commensurate $\sqrt{7} \times \sqrt{7}$ lateral periodicity of graphene and 2×2 lateral periodicity of the WS₂ surface, is used (see Fig. 1a). A vacuum layer of more than 20\AA in thickness is inserted in the direction normal to the layers between supercells. After structural relaxation, graphene layers maintain their planar and hexagonal atomic network and the average distance between the graphene layer and the sulfur atoms in the first WS₂ layer is about 3.50\AA (see Fig. 1a).

Results and Discussion

Free-standing graphene is a zero-gap semimetal whose conduction and valence bands meet at the Dirac point. Pure WS_2 exhibits semiconducting character with a band gap changing from direct (monolayer ~ 2.1 eV) to indirect (bulk ~ 1.4 eV).¹ In Fig. 1b we show the band structure of a Gr/monolayer WS_2 /Gr sandwich along high symmetry k directions of the WS_2 supercell. The Dirac point of the two graphene layers appear within the energy gap of WS_2 , and the linear bands around the Dirac point of free-standing graphene are preserved due to the weak van der Waals (vdW) interaction between graphene and WS_2 .³⁵ Similar to a single graphene sheet, the sandwich system also has a low density of states (DOS) around the Fermi level making it easy to move the Fermi level by a gate voltage. The conduction band minimum (CBM) and the valence band maximum (VBM) of WS_2 at K point defines the band gap (E_{gk}) of WS_2 . The energy difference between the CBM and the Fermi level is defined as the effective tunneling barrier height, ΔE , an important parameter in electron tunneling for FET (see Fig. 1b). The energy splitting of the valence band at K point (E_{so}) due to the strong spin-orbit coupling in WS_2 ^{36,37} is also indicated in Fig. 1b.

Thickness, Gate Field Effects and ON/OFF ratio. As informed by experiment,²⁴ the ON/OFF ratio changes with the number of WS_2 layers in a Gr/ WS_2 /Gr junction. We first examine band structure evolution with the WS_2 layer thickness. Figure 2a shows how ΔE , E_{gk} and E_{so} change with the number of WS_2 layers. The change in the band gap E_{gk} with the number of WS_2 layers is from the quantum confinement effect.³⁸ The effective tunneling barrier height ΔE trends with E_{gk} (see Fig. 2a), which should affect electron tunneling. On the other hand, the splitting of the valence band top due to the spin-orbit coupling (E_{so}) shows an opposite trend with the number of WS_2 layers.

The effect of the gate field is equivalent to doping the hybrid system. Positive gate field corresponds to electron doping and negative gate field hole doping. The gate field modifies the barrier height (ΔE) by moving the Fermi level of the system relative to the conduction band bottom of the WS_2 layer. Figure 2b shows the evolution of ΔE as a function of the electric displacement field D_g for different number of WS_2 layers. Specifically, electron doping moves the Fermi level of the

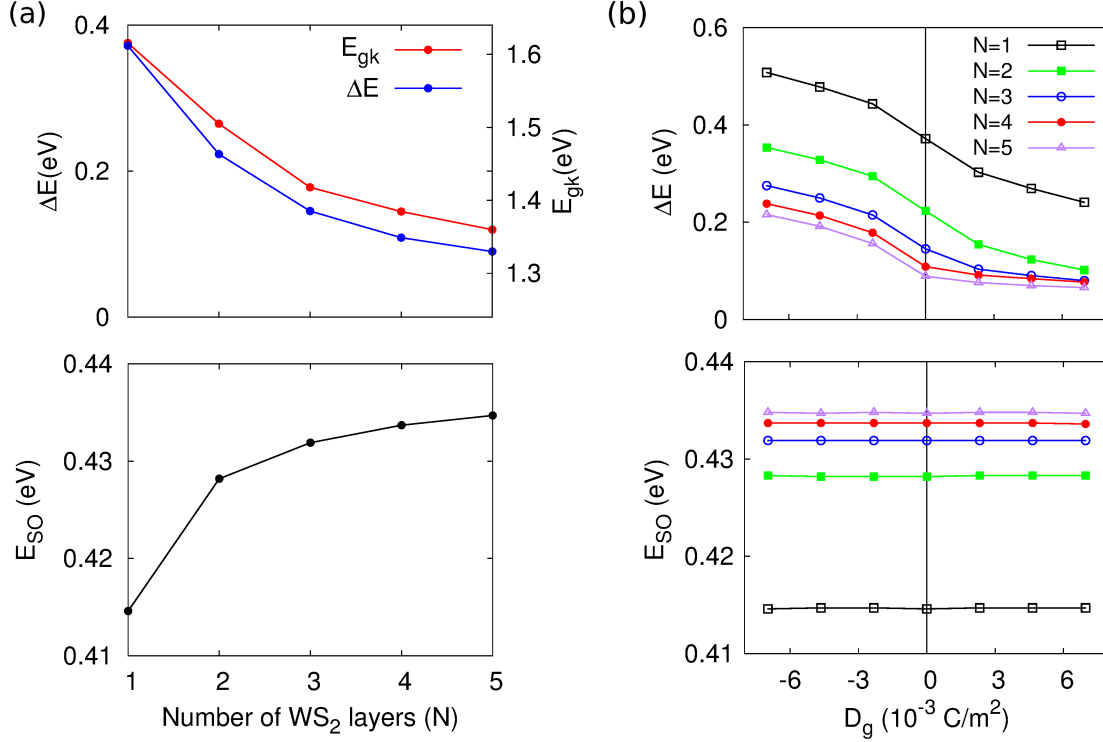


Figure 2: The effect of gate field and WS_2 layer thickness on the electronic properties of the Gr/ WS_2 /Gr hybrid system. The band gap of WS_2 at K (E_{gk}), effective tunneling barrier height (ΔE) and energy splittings of valence band at K due to the spin-orbit coupling in WS_2 as a function of (a) the number of WS_2 layers and (b) the gate field D_g for different number of WS_2 layers. N denotes the number of WS_2 layers .

system closer to the CBM of the WS_2 layer making ΔE decreased at positive gate field and vice versa. The rate of change slightly decreases at higher field (large D_g) because of the increased DOS at the Fermi energy in graphene as the Fermi energy is moved away from the Dirac point by the gate field. When the WS_2 layer is thin enough (N=1, 2), the change in ΔE is symmetric for positive and negative gate field. As the thickness of WS_2 increases, ΔE changes by a much smaller amount under a positive gate field than under a negative gate field, making the curve non-symmetric any more. This is because when the thickness of WS_2 increases, the Dirac point of graphene gets closer to the CBM of WS_2 (ΔE getting smaller, see Figure 2a). Further reducing ΔE by applying a gate field can make ΔE comparable to the gaussian smearing (0.05 eV) for the energy levels (in reality, a similar effect is achieved by thermal smearing). As a result, some of the conduction states of WS_2 can be occupied impeding any further movement of the Fermi level. There is no such effect

for negative gate field since under a negative gate field, the Fermi level moves farther away from the CBM of WS₂. Thus the change in ΔE under negative gate field is almost the same for different thickness of WS₂ (see Figure 2b). We can also see that within the experimental gate field range (limited by the gate dielectric breakdown), the maximum change in ΔE is about 0.25 eV.

The gate field has little effect on E_{so} . This is because the two valence bands at K are both mostly d states from W atoms³⁸ and as the gate field is applied, the shift in the potential for these states are the same.

To relate our first-principles calculation with experiments, we employ a simple tunneling formula³⁹⁻⁴¹ (see Part “Current-Voltage Characteristics”), using first-principles results as input, to calculate the tunneling current as a function of the gate voltage. The obtained I-V characteristics can then be compared with experimental data. When there are four layers of WS₂ in the hybrid system ($N = 4$), our calculated result predicts an ON/OFF ratio approaching 1000, close to experimental measurement. The calculated I-V curve compared with experiment are included in Part “Current-Voltage Characteristics”.

Dielectric properties. Graphene based FETs have been widely studied by combining experimental measurements and macroscopic electrostatic models.^{19,42,43} In these models, the dielectric barrier between the graphene layers is treated as a region with a constant dielectric permittivity equal to the bulk value. However, interfaces can have significantly different dielectric properties than the bulk.⁴⁴

In general, the electric displacement field D is related to the electric field E and the polarization P in the following form

$$D = \epsilon_0 E + P, \quad (1)$$

where ϵ_0 is the electric permittivity of the vacuum. P can be expressed as the summation over centers of Wannier functions according to the modern theory of polarization,^{45,46} and in principle includes all dielectric properties of the medium. To calculate P we follow the method in Ref.[

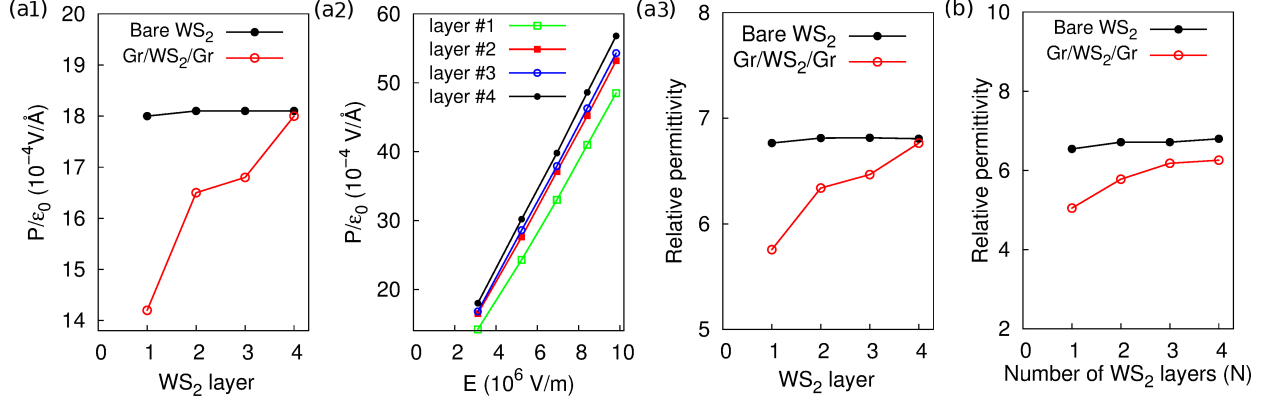


Figure 3: Dielectric properties of the Gr/WS₂/Gr hybrid system compared with bare WS₂ system. In **(a1-a3)**, we focus on the dielectric properties of the Gr/WS₂/Gr hybrid system with a fixed WS₂ thickness (four layer WS₂). The calculated local polarization in each WS₂ layer **(a1)** induced by an gate field of $D_g = 4.65 \times 10^{-4}$ C/m², which produces an electric field of $E = 3.12 \times 10^6$ V/m within the WS₂ layer (red), along with data of bare WS₂ (without graphene electrodes, black) for comparison, and **(a2)** as a function of the electric field (E) in WS₂. **(a3)** The calculated local effective relative dielectric constant in each WS₂ layer. Layer 4 is closest to the gate. In **(b)**, we considers Gr/WS₂/Gr hybrid system with different WS₂ thickness. It shows the calculated total effective relative dielectric constant of the Gr/WS₂/Gr sandwich and bare WS₂ (black) as a function of WS₂ layer thickness.

34]. The calculated polarization of the WS₂ layers adjacent to the graphene layers is found to be different than that of the inner WS₂ layers. This contrasts the case of the WS₂ film without the graphene layers, in which the polarization is nearly the same across different WS₂ layers (see Fig. 3a1), or the case of the Gr/*h*-BN/Gr system, in which the interface with graphene layers has little effect on the dielectric properties of the *h*-BN thin layers.³⁴ In the Gr/WS₂/Gr junction, the effect of the interface on the dielectric constant extends to several layers of WS₂.

The gate field effect on the polarization of each WS₂ layer is shown in Fig. 3a2. The linearity of all the curves allow us to extract the dielectric constant,

$$\epsilon = 1 + \frac{P}{\epsilon_0 E}, \quad (2)$$

where E is equal to the slope of the self-consistent Kohn-Sham effective potential perpendicular to the junction. The dielectric constant in each layer of WS₂ extracted from this expression using the local polarization is plotted in Fig. 3a3. We can also extract a total effective dielectric constant

from the total polarization. In Fig. 3b we plot the total dielectric constant as a function of the thickness of the WS₂ layer, and compare to that of bare WS₂. Since the total dielectric constant is essentially the average of the layer dielectric constant, it shows a similar thickness dependence as that of individual layers. The result shows a significant reduction of the dielectric constant of the WS₂ layer due to its interface with graphene. This contrasts sharply with the Gr/h-BN/Gr system, where the dielectric constant is almost layer independent.³⁴

Current-Voltage Characteristics. The tunneling formula we employ to calculate the tunneling current explicitly includes the density of states of both the top (T) and bottom (B) graphene electrode layers,

$$\rho_{T(B)}(E) = \frac{2|E|}{\pi\hbar^2 V_F^2}. \quad (3)$$

Placing the zero-bias chemical potential of the system at $E = 0$ and assuming symmetric potential shifts of $\pm eV/2$ for the two electrodes upon applying a bias voltage, the current density is given by,

$$\begin{aligned} J(V) &= C \int \rho_B \left(E + \frac{eV}{2} - E_{DB} \right) \rho_T \left(E - \frac{eV}{2} - E_{DT} \right) \\ &\times \left[f \left(E - \frac{eV}{2} \right) - f \left(E + \frac{eV}{2} \right) \right] T(E) dE, \end{aligned} \quad (4)$$

where C is a constant, $E_{DT(B)}$ are the energy at the Dirac point of the top (bottom) electrode measured from the chemical potential,

$$f(E) = \frac{1}{e^{E/k_B T} + 1} \quad (5)$$

is the Fermi distribution function, and

$$T(E) = \begin{cases} \exp \left[-\frac{2d_{barrier}}{\hbar} \sqrt{2m^*(\Delta E - E)} \right], & E < \Delta E; \\ 1, & E > \Delta E. \end{cases} \quad (6)$$

is the transmission probability with an exponential form using the WKB approximations.⁴⁷ The effective mass m^* ($\sim 0.48 m_0$, m_0 is the free electron mass) of an electron along the transport direction in WS₂ can be obtained from the band structure calculations. The barrier width $d_{barrier}$

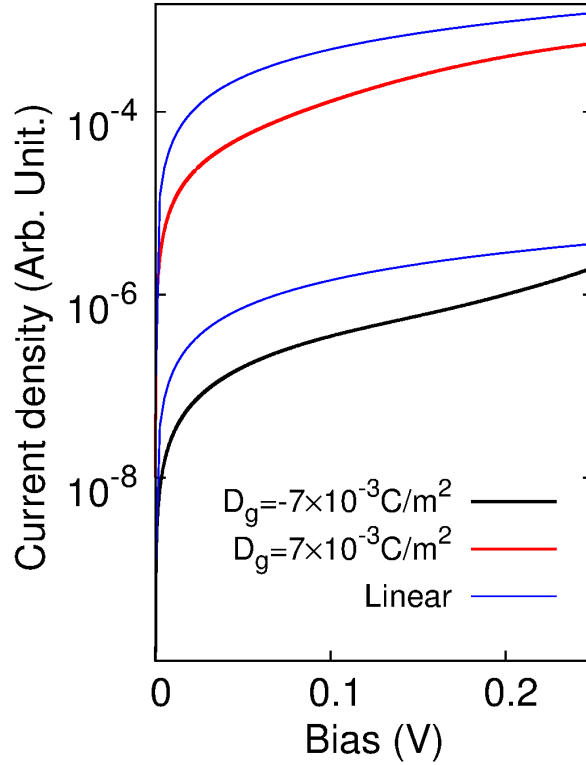


Figure 4: Current density under different gate fields D_g (semi-logarithmic scale) with $N = 4$. Positive (negative) D_g corresponds to the ON (OFF) state. The ON state (red) curve is nearly linear, as it closely tracks a linear function (blue curve) plotted as a guide. $T = 300$ K .

is taken as the distance between the two graphene electrodes, and the effective barrier height ΔE and the energy of Dirac point E_D are extracted from the first-principles calculations. The fermi velocity V_F of graphene is a constant.

Equation (4) neglects in-plane momentum conservation, an approximation which is valid if inter-valley tunneling (i.e., incident and transmitted wave functions belong to different K valleys in the 2D Brillouine zone) does not make a significant contribution. The other limit in which one can neglect momentum conservation is the limit of strong interface disorder, for example when the lattice mismatch between the layers introduces sufficient defects at the interface such that coherent momentum conserving transmission is not possible.³⁹ Even though in both scenarios the formula takes the same form, the constant prefactor C for these two cases is different. We focus on the qualitative characteristics of the I-V curve, the determination of the value of prefactor C is still an open question (see supporting information).

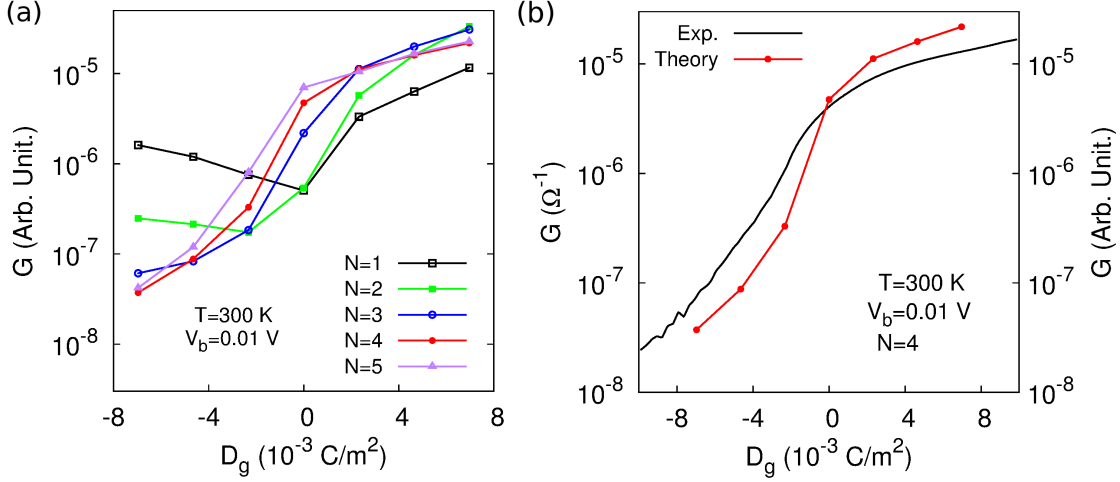


Figure 5: (Color online) Conductance-gate field plot at $T=300 \text{ K}$, bias voltage $V_b = 0.01 \text{ V}$ (a) calculated for different number (N) of WS_2 layers, and (b) experimental data for $N = 4$ compared to theory.

The above model yields the current density as a function of the bias voltage under different electric displacement fields D_g (gate field) and the low bias conductance as a function of the gate field D_g as plotted in Figs. 4 and 5, respectively. Take as example the case of $N = 4$, for which experimental data is available. The calculated I-V curves are shown in Fig. 4. The device is in the ON state when the gate field is $D_g = 7 \times 10^{-3} \text{ C/m}^2$, evident from both a large current and a nearly linear I-V curve. A negative gate field raises the tunnel barrier and keeps the device in the OFF state as evident from greatly reduced current and a nonlinear I-V curve. The low bias conductance as a function of gate field D_g and number of layers of WS_2 in Fig. 5a shows different trends for positive and negative gate fields. At negative gate fields, the barrier is high so the dominant variable in the conductance is the WS_2 thickness, which causes the conductance to decrease with the increasing thickness. At positive gate fields, the barrier height is greatly reduced and increasing WS_2 thickness causes further reduction of the barrier height when WS_2 layer is thin ($N = 1$ and $N = 2$) leading to an increase in the conductance. This trend is reversed for $N > 2$, because at these thicknesses the Fermi level is so close to the CBM of WS_2 (comparable to the gaussian smearing), increasing WS_2 thickness can not further reduce the barrier height (the change of ΔE is asymmetric in Figure 2b) under positive gate fields. For very thin WS_2 thicknesses ($N = 1$ and

$N = 2$), a third competing factor, the DOS of the two graphene electrodes, comes into play. As the gate field is increased from zero in either positive or negative directions, the Fermi energy DOS increases linearly from zero. Therefore the low bias conductance also increases if all other factors remain unchanged. This is indeed the case for $N = 1$, which shows a turning point at $D_g = 0$ in Fig. 5a, and somewhat true for $N = 2$, with a turning point at a slightly negative D_g .

To compare with experimental data, we plot both simulation and experimental curves for $N = 4$ in Fig. 5b. The two curves agree very well.

CONCLUSION

First-principles calculations of the electronic structures of Gr/WS₂/Gr field-effect transistors show that the effective barrier height of WS₂ in contact with graphene decreases with increasing number of WS₂ layers, and can be tuned by a gate field. A transport model built on top of the first-principles calculations show that the ON/OFF ratio is size-dependent and reaches a significant high value with an appropriate number of WS₂ layers and a suitable range of gate voltages. The spin-orbit effect in WS₂ has also been investigated and it has a slight layer dependence, but is independent of the gate field. Comparison of the dielectric constant of bare WS₂ and Gr/WS₂/Gr sandwiches shows that interfacing with graphene can significantly reduce the dielectric constant of WS₂ and the effect gradually decreases as the number of WS₂ layers increases. The effects of the barrier layer thickness and the gate field on the transport properties of Gr/WS₂/Gr FET are clearly connected to the band structure change as shown from first-principles calculations, providing important information for future nanoelectronic device design.

Acknowledgement

This work was supported by the US Department of Energy (DOE), Office of Basic Energy Sciences (BES), under Contract No. DE-FG02-02ER45995. The computation was done using the utilities

of the National Energy Research Scientific Computing Center (NERSC).

Supporting Information Available: This material is available free of charge via the Internet at <http://pubs.acs.org>.

References

- (1) Qinghua, W.; Kourosh, K.; Andras, K.; Jonathan, N. C.; Michael, S. S. Electronics and optoelectronics of two-dimensional transition metal dichalcogenides. *Nat Nano* **2012**, *7*, 699.
- (2) Zhao, W.; Ghorannevis, Z.; Chu, L.; Toh, M.; Kloc, C.; Tan, P.-H.; Eda, G. Evolution of Electronic Structure in Atomically Thin Sheets of WS₂ and WSe₂. *ACS Nano* **2013**, *7*, 791–797.
- (3) Xiao, D.; Liu, G.-B.; Feng, W.; Xu, X.; Yao, W. Coupled Spin and Valley Physics in Monolayers of MoS₂ and Other Group-VI Dichalcogenides. *Phys. Rev. Lett.* **2012**, *108*, 196802.
- (4) Mak, K. F.; He, K.; Shan, J.; Heinz, T. F. Control of valley polarization in monolayer MoS₂ by optical helicity. *Nat Nano* **2012**, *7*, 494.
- (5) He, J.; Hummer, K.; Franchini, C. Stacking effects on the electronic and optical properties of bilayer transition metal dichalcogenides MoS₂, MoSe₂, WS₂, and WSe₂. *Physical Review B* **2014**, *89*, 075409.
- (6) Li, Y.; Chernikov, A.; Zhang, X.; Rigosi, A.; Hill, H. M.; van der Zande, A. M.; Chenet, D. A.; Shih, E.-M.; Hone, J.; Heinz, T. F. Measurement of the optical dielectric function of monolayer transition-metal dichalcogenides: MoS₂, MoSe₂, WS₂, and WSe₂. *Physical Review B* **2014**, *90*, 205422.
- (7) Johari, P.; Shenoy, V. B. Tuning the electronic properties of semiconducting transition metal dichalcogenides by applying mechanical strains. *ACS nano* **2012**, *6*, 5449–5456.

- (8) Muratore, C.; Varshney, V.; Gengler, J.; Hu, J.; Bultman, J.; Smith, T.; Shamberger, P.; Qiu, B.; Ruan, X.; Roy, A. Cross-plane thermal properties of transition metal dichalcogenides. *Applied Physics Letters* **2013**, *102*, 081604.
- (9) Wu, D.; Pak, A. J.; Liu, Y.; Zhou, Y.; Wu, X.; Zhu, Y.; Lin, M.; Han, Y.; Ren, Y.; Peng, H.; Tsai, Y.-H.; Hwang, G. S.; Lai, K. Thickness-Dependent Dielectric Constant of Few-Layer In₂Se₃ Nanoflakes. *Nano Letters* **2015**, *15*, 8136–8140.
- (10) Zeng, H.; Liu, G.; Dai, J.; Yan, Y.; Zhu, B.; He, R.; Xie, L.; Xu, S.; Chen, X.; Yao, W. Optical signature of symmetry variations and spin-valley coupling in atomically thin tungsten dichalcogenides. *Scientific Reports* **2013**, *3*, 1608.
- (11) Novoselov, K. S.; Geim, A. K.; Morozov, S. V.; Jiang, D.; Zhang, Y.; Dubonos, S. V.; Grigorieva, I. V.; Firsov, A. A. Electric Field Effect in Atomically Thin Carbon Films. *Science* **2004**, *306*, 666–669.
- (12) Lin, M.-W.; Ling, C.; Zhang, Y.; Yoon, H. J.; Cheng, M. M.-C.; Agapito, L. A.; Kioussis, N.; Widjaja, N.; Zhou, Z. Room-temperature high on/off ratio in suspended graphene nanoribbon field-effect transistors. *Nanotechnology* **2011**, *22*, 265201.
- (13) Li, X.; Wang, X.; Zhang, L.; Lee, S.; Dai, H. Chemically Derived, Ultrasoft Graphene Nanoribbon Semiconductors. *Science* **2008**, *319*, 1229–1232.
- (14) Han, M. Y.; Özyilmaz, B.; Zhang, Y.; Kim, P. Energy Band-Gap Engineering of Graphene Nanoribbons. *Phys. Rev. Lett.* **2007**, *98*, 206805.
- (15) Balog, R. et al. Bandgap opening in graphene induced by patterned hydrogen adsorption. *Nat Mater* **2010**, *9*, 315.
- (16) Elias, D. C.; Nair, R. R.; Mohiuddin, T. M. G.; Morozov, S. V.; Blake, P.; Halsall, M. P.; Ferrari, A. C.; Boukhvalov, D. W.; Katsnelson, M. I.; Geim, A. K.; Novoselov, K. S. Control of

- Graphene's Properties by Reversible Hydrogenation: Evidence for Graphane. *Science* **2009**, 323, 610–613.
- (17) Yuanbo, Z.; Tsung-Ta, T.; Caglar, G.; Zhao, H.; Michael, C. M.; Alex, Z.; Michael, F. C.; Ron, Y. S.; Feng, W. Direct observation of a widely tunable bandgap in bilayer graphene. *Nature* **2009**, 459, 820.
- (18) Jeroen, B. O.; Hubert, B. H.; Xinglan, L.; Alberto, F. M.; Lieven M, K. V. Gate-induced insulating state in bilayer graphene devices. *Nat Mater* **2008**, 7, 151.
- (19) Britnell, L.; Gorbachev, R. V.; Jalil, R.; Belle, B. D.; Schedin, F.; Mishchenko, A.; Georgiou, T.; Katsnelson, M. I.; Eaves, L.; Morozov, S. V.; Peres, N. M. R.; Leist, J.; Geim, A. K.; Novoselov, K. S.; Ponomarenko, L. A. Field-Effect Tunneling Transistor Based on Vertical Graphene Heterostructures. *Science* **2012**, 335, 947–950.
- (20) Sciambi, A.; Pelliccione, M.; Lilly, M. P.; Bank, S. R.; Gossard, A. C.; Pfeiffer, L. N.; West, K. W.; Goldhaber-Gordon, D. Vertical field-effect transistor based on wave-function extension. *Phys. Rev. B* **2011**, 84, 085301.
- (21) Zaslavsky, A.; Aydin, C.; Luryi, S.; Cristoloveanu, S.; Mariolle, D.; Fraboulet, D.; Deleonibus, S. Ultrathin silicon-on-insulator vertical tunneling transistor. *Applied Physics Letters* **2003**, 83, 1653–1655.
- (22) Braga, D.; Lezama, I. G.; Berger, H.; Morpurgo, A. F. Quantitative Determination of the Band Gap of WS₂ with Ambipolar Ionic Liquid-Gated Transistors. *Nano Letters* **2012**, 12, 5218–5223.
- (23) Zhao, W.; Ghorannevis, Z.; Chu, L.; Toh, M.; Kloc, C.; Tan, P.-H.; Eda, G. Evolution of Electronic Structure in Atomically Thin Sheets of WS₂ and WSe₂. *ACS Nano* **2013**, 7, 791–797.

- (24) Thanasis, G.; Rashid, J.; Branson, D. B.; Liam, B.; Roman, V. G.; Sergey, V. M.; Yong-Jin, K.; Ali, G.; Sarah, J. H.; Oleg, M.; Laurence, E.; Leonid, A. P.; Andre, K. G.; Kostya, S. N.; Artem, M. Vertical field-effect transistor based on graphene-WS₂ heterostructures for flexible and transparent electronics. *Nat Nano* **2013**, *8*, 100.
- (25) Chhowalla, M.; Shin, H. S.; Eda, G.; Li, L.-J.; Loh, K. P.; Zhang, H. The chemistry of two-dimensional layered transition metal dichalcogenide nanosheets. *Nature chemistry* **2013**, *5*, 263–275.
- (26) Yun, W. S.; Han, S. W.; Hong, S. C.; Kim, I. G.; Lee, J. D. Thickness and strain effects on electronic structures of transition metal dichalcogenides: 2H-MX₂ semiconductors ($M = \text{Mo}, \text{W}; X = \text{S}, \text{Se}, \text{Te}$). *Phys. Rev. B* **2012**, *85*, 033305.
- (27) Conley, H. J.; Wang, B.; Ziegler, J. I.; Richard F. Haglund, J.; Pantelides, S. T.; Bolotin, K. I. Bandgap Engineering of Strained Monolayer and Bilayer MoS₂. *Nano Letters* **2013**, *13*, 3626–3630.
- (28) Kohn, W.; Sham, L. J. Self-Consistent Equations Including Exchange and Correlation Effects. *Phys. Rev.* **1965**, *140*, A1133–A1138.
- (29) Giannozzi, P. et al. QUANTUM ESPRESSO: a modular and open-source software project for quantum simulations of materials. *Journal of Physics: Condensed Matter* **2009**, *21*, 395502.
- (30) Blöchl, P. E.; Jepsen, O.; Andersen, O. K. Improved tetrahedron method for Brillouin-zone integrations. *Phys. Rev. B* **1994**, *49*, 16223–16233.
- (31) Kresse, G.; Joubert, D. From ultrasoft pseudopotentials to the projector augmented-wave method. *Phys. Rev. B* **1999**, *59*, 1758–1775.
- (32) Klimeš, J.; Bowler, D. R.; Michaelides, A. Van der Waals density functionals applied to solids. *Phys. Rev. B* **2011**, *83*, 195131.

- (33) Otani, M.; Sugino, O. First-principles calculations of charged surfaces and interfaces: A plane-wave nonrepeated slab approach. *Phys. Rev. B* **2006**, *73*, 115407.
- (34) Wang, Y.-P.; Cheng, H.-P. First-principles simulations of a graphene-based field-effect transistor. *Phys. Rev. B* **2015**, *91*, 245307.
- (35) Li, S.-S.; Zhang, C.-W. First-principles study of graphene adsorbed on WS₂ monolayer. *Journal of Applied Physics* **2013**, *114*.
- (36) Kormányos, A.; Zólyomi, V.; Drummond, N. D.; Burkard, G. Spin-Orbit Coupling, Quantum Dots, and Qubits in Monolayer Transition Metal Dichalcogenides. *Phys. Rev. X* **2014**, *4*, 011034.
- (37) Zhu, Z. Y.; Cheng, Y. C.; Schwingenschlögl, U. Giant spin-orbit-induced spin splitting in two-dimensional transition-metal dichalcogenide semiconductors. *Phys. Rev. B* **2011**, *84*, 153402.
- (38) Kuc, A.; Zibouche, N.; Heine, T. Influence of quantum confinement on the electronic structure of the transition metal sulfide TS₂. *Phys. Rev. B* **2011**, *83*, 245213.
- (39) Britnell, L.; Gorbachev, R. V.; Jalil, R.; Belle, B. D.; Schedin, F.; Katsnelson, M. I.; Eaves, L.; Morozov, S. V.; Mayorov, A. S.; Peres, N. M. R.; Neto, A. H. C.; Leist, J.; Geim, A. K.; Ponomarenko, L. A.; Novoselov, K. S. Electron Tunneling through Ultrathin Boron Nitride Crystalline Barriers. *Nano Letters* **2012**, *12*, 1707–1710.
- (40) Simmons, J. G. Generalized Formula for the Electric Tunnel Effect between Similar Electrodes Separated by a Thin Insulating Film. *Journal of Applied Physics* **1963**, *34*, 1793–1803.
- (41) Wolf, E. L. *Principles of electron tunneling spectroscopy*; OUP Oxford, 2011.
- (42) Ponomarenko, L. A.; Belle, B. D.; Jalil, R.; Britnell, L.; Gorbachev, R. V.; Geim, A. K.; Novoselov, K. S.; Castro Neto, A. H.; Eaves, L.; Katsnelson, M. I. Field-effect control of tunneling barrier height by exploiting graphene's low density of states. *Journal of Applied Physics* **2013**, *113*, 136502.

- (43) Bala Kumar, S.; Seol, G.; Guo, J. Modeling of a vertical tunneling graphene heterojunction field-effect transistor. *Applied Physics Letters* **2012**, *101*, 033503.
- (44) Giustino, F.; Umari, P.; Pasquarello, A. Dielectric Discontinuity at Interfaces in the Atomic-Scale Limit: Permittivity of Ultrathin Oxide Films on Silicon. *Phys. Rev. Lett.* **2003**, *91*, 267601.
- (45) King-Smith, R. D.; Vanderbilt, D. Theory of polarization of crystalline solids. *Phys. Rev. B* **1993**, *47*, 1651–1654.
- (46) Resta, R. Macroscopic polarization in crystalline dielectrics: the geometric phase approach. *Rev. Mod. Phys.* **1994**, *66*, 899–915.
- (47) Bender, C. M.; Orszag, S. A. *Advanced mathematical methods for scientists and engineers I: Asymptotic Methods and Perturbation Theory*; Springer Science & Business Media, 1999.